

Crystallite size and phase purity in $\text{Pb}_{1-x}\text{Sr}_x\text{TiO}_3$ ferroelectric perovskites for biomedical applications via controlled sintering

Rahmat Doni Widodo, Samsudin Anis, Deni Fajar Fitriyana, Maykel Manawan, Joni Sah, Aji Santiko, Rizalman Bin Mamat, Abdulfatah Abdu Yusuf & Muhammad Imam Ammarullah

To cite this article: Rahmat Doni Widodo, Samsudin Anis, Deni Fajar Fitriyana, Maykel Manawan, Joni Sah, Aji Santiko, Rizalman Bin Mamat, Abdulfatah Abdu Yusuf & Muhammad Imam Ammarullah (2024) Crystallite size and phase purity in $\text{Pb}_{1-x}\text{Sr}_x\text{TiO}_3$ ferroelectric perovskites for biomedical applications via controlled sintering, Journal of Asian Ceramic Societies, 12:4, 332-343, DOI: [10.1080/21870764.2024.2421046](https://doi.org/10.1080/21870764.2024.2421046)

To link to this article: <https://doi.org/10.1080/21870764.2024.2421046>



© 2024 The Author(s). Published by Informa UK Limited, trading as Taylor & Francis Group on behalf of The Korean Ceramic Society and The Ceramic Society of Japan.



Published online: 27 Oct 2024.



Submit your article to this journal [↗](#)



Article views: 174






View related articles [↗](#)



View Crossmark data [↗](#)

Crystallite size and phase purity in $\text{Pb}_{1-x}\text{Sr}_x\text{TiO}_3$ ferroelectric perovskites for biomedical applications via controlled sintering

Rahmat Doni Widodo ^a, Samsudin Anis ^a, Deni Fajar Fitriyana ^{a,b}, Maykel Manawan ^{c,d}, Joni Sah ^c, Aji Santiko^a, Rizalman Bin Mamat ^{e,f}, Abdulfatah Abdu Yusuf ^{g,h} and Muhammad Imam Ammarullah ^{b,h,i}

^aDepartment of Mechanical Engineering, Faculty of Engineering, Universitas Negeri Semarang, Semarang, Central Java, Indonesia;

^bDepartment of Mechanical Engineering, Faculty of Engineering, Universitas Diponegoro, Semarang, Central Java, Indonesia; ^cResearch Center for Advanced Material, National Research and Innovation Agency (BRIN), South Tangerang, Banten, Indonesia; ^dFaculty of Defense Science and Technology, Universitas Pertahanan Indonesia, Bogor, West Java, Indonesia; ^eFaculty of Mechanical & Automotive Engineering Technology, Universiti Malaysia Pahang Al-Sultan Abdullah, Pekan, Pahang, Malaysia; ^fCentre for Automotive Engineering, Universiti Malaysia Pahang Al-Sultan Abdullah, Pekan, Pahang, Malaysia; ^gDepartment of Mechanical Engineering, College of Engineering, University of Liberia, Monrovia, Montserrado, Liberia; ^hSustainable Energy and Bioengineering Research Centre, University of Liberia, Monrovia, Montserrado, Liberia; ⁱUndip Biomechanics Engineering & Research Centre (UBM-ERC), Universitas Diponegoro, Semarang, Central Java, Indonesia

ABSTRACT

Lead strontium titanate ($\text{Pb}_{1-x}\text{Sr}_x$) TiO_3 (PST) is a ferroelectric perovskite material with tunable properties, including Curie temperature, spontaneous polarization, and high dielectric permittivity, making it promising for advanced biomedical applications, such as biosensors, bioimaging, and light-activated therapeutics. This study investigates the effect of varying sintering temperatures on the crystallite size and phase purity of PST, aiming to optimize its performance for biomedical devices. PbCO_3 , SrCO_3 , and TiO_2 powders were processed via ball milling for 58 hours, followed by sintering at temperatures ranging from 500°C to 1100°C. Laser diffraction particle size analysis and X-ray diffraction (XRD) were used to assess the particle size and crystal phase transformations. The results demonstrate that higher sintering temperatures improve the PST phase composition, reducing impurities and enhancing crystallite growth. The most significant crystal growth was observed at 900°C, while the optimal phase purity and crystallite size (91.5 nm) were achieved at 1100°C, producing 100% single-phase PST. These findings emphasize the critical role of sintering temperature in tailoring PST's properties, enhancing its suitability for electronic and microelectronic biomedical devices. Controlled sintering in perovskite materials opens new pathways for their application in medical diagnostics and therapeutic technologies.

ARTICLE HISTORY

Received 27 August 2024
Accepted 17 October 2024

KEYWORDS





Lead strontium titanate; perovskite; PbTiO_3 ; SrCO_3 ; TiO_2

1. Introduction

Lead strontium titanate ($\text{Pb}_{1-x}\text{Sr}_x$) TiO_3 (PST), like the widely studied Barium Strontium Titanate (BST), is a ferroelectric perovskite material that holds significant promise for both electronic and biomedical applications due to its unique tunable properties [1]. PST is a solid solution composed of lead titanate (PbTiO_3 , P.T.) and strontium titanate (SrTiO_3 , S.T.), which allows for precise control over its physical characteristics, such as Curie temperature, spontaneous polarization, and dielectric permittivity, making it particularly attractive for biosensors, bioimaging, and light-activated therapeutic devices [2,3]. At room temperature, P.T. exhibits a tetragonal structure with high spontaneous polarization and a high Curie temperature of 490°C, while S.T. has a cubic paraelectric structure with a much lower Curie temperature of -167°C [3,4]. By adjusting the ratio of P.T. and S.T., the Curie temperature of PST can be finely tuned, offering tailored functionality for various biomedical devices.

Research shows that increasing the Sr²⁺ content in the PST solid solution decreases the Curie temperature linearly while increasing the lattice volume and tetragonality, resulting in tunable phase transitions and enhanced material properties [5,6]. When the Sr content is below 0.60, the PST solid solution exhibits a ferroelectric phase, while higher Sr concentrations (0.60–1.00) induce a paraelectric phase at room temperature [1,5–7]. These properties, including excellent spontaneous polarization, high dielectric permittivity, and tunability, make PST an attractive material for applications requiring precise thermal and electrical responsiveness [8,9]. Moreover, PST's single-phase transition and higher reproducibility, compared to other perovskites such as BST, make it highly suitable for biomedical sensors and devices that require consistent performance and reliability [6,10].

PST's low crystallization temperature and high tunability reduce issues such as substrate-film diffusion,

CONTACT Rahmat Doni Widodo  rahmat.doni@mail.unnes.ac.id  Department of Mechanical Engineering, Faculty of Engineering, Universitas Negeri Semarang, Semarang, Central Java 50229, Indonesia; Muhammad Imam Ammarullah  imamammarullah@gmail.com  Department of Mechanical Engineering, Faculty of Engineering, Universitas Diponegoro, Semarang, Central Java 50275, Indonesia

© 2024 The Author(s). Published by Informa UK Limited, trading as Taylor & Francis Group on behalf of The Korean Ceramic Society and The Ceramic Society of Japan. This is an Open Access article distributed under the terms of the Creative Commons Attribution License (<http://creativecommons.org/licenses/by/4.0/>), which permits unrestricted use, distribution, and reproduction in any medium, provided the original work is properly cited. The terms on which this article has been published allow the posting of the Accepted Manuscript in a repository by the author(s) or with their consent.

which is crucial for developing tunable biomedical devices like biosensors, piezoelectric sensors, and transducers [10]. These features have led to the widespread use of PST in electronics, where it is used in devices such as field-effect transistors (FET-FeRAM), dielectric capacitors, and tunable microwave devices [1,5–12]. More recently, its properties have also been harnessed in biomedical technologies, where PST's piezoelectric and ferroelectric behavior can be applied to bioimaging, light-activated therapeutic technologies, and biosensing applications, offering new possibilities in medical diagnostics and treatments [13].

While significant research has been conducted on PST ceramics with varying Pb/Sr ratios, additional studies are needed to optimize its properties for biomedical use. The sintering process plays a critical role in controlling the crystallite size and phase purity, which directly affect PST's functional properties. PST materials can be synthesized using several methods, including sol-gel, hydrothermal, and solid-state reactions, with the solid-state reaction method being particularly advantageous due to its simplicity, scalability, and ability to produce homogeneous, high-purity materials [14,15]. The solid-state reaction method allows for precise control over particle size and crystallinity, which are essential for biomedical applications where material consistency and phase purity are critical [16,17]. The solid-state reaction is the predominant technique for generating polycrystalline solid solutions from a blend of solid substances [18]. PST can be synthesized using this method with different metal oxide precursors [18,19]. However, the reactions generally require high temperatures for the PST formation process to occur at an acceptable rate [18]. PST production can typically be accomplished by heating within a range of 400 to 1250°C for varying durations [4,20,21].

In this study, the authors report the preparation of PST powder from a mixture of PbCO_3 , SrCO_3 , and TiO_2 using the solid-state reaction method and subsequent sintering process to investigate the effect of sintering temperature on the weight percentage and crystallite size of the resulting PST material. By tuning these parameters, present study aim to optimize PST's properties for potential applications in biomedical devices such as biosensors and bioimaging systems. Sintering temperatures ranging from 500°C to 1100°C were applied to achieve high phase purity and controlled crystallite size, thus enhancing PST's performance for medical applications that require precise material

properties. The results provide valuable insights into the optimal processing conditions for producing high-quality PST materials for biomedical technologies.

2. Materials and methods

The synthesis of PST ferroelectric perovskite was carried out using high-purity powders of PbCO_3 , SrCO_3 , and TiO_2 (99% purity, Sigma-Aldrich), as summarized in Table 1. The specific masses of PbCO_3 (34.65 g), SrCO_3 (28.72 g), and TiO_2 (25.89 g) were weighed according to the stoichiometric requirements of the target composition. The powders were homogenized through vibratory ball milling for 58 hours to ensure a consistent blend and a uniform distribution of components. The milling was performed at 900 rpm, utilizing a ball-to-powder weight ratio of 10:1 with 10 mL of alcohol as a milling medium to reduce particle agglomeration and promote effective mixing. This ball milling process helps to reduce the particle size of the raw materials, which is critical for improving sinterability and enhancing phase purity in the final PST material.

To monitor particle size reduction and phase evolution, X-Ray Diffraction (XRD) and Particle Size Analyzer (P.S.A.) measurements were taken before and after milling at intervals of 5, 10, 25, 35, 45, and 55 hours. These analyses provided insights into the phase homogeneity and particle size distribution during the milling process, ensuring optimal starting conditions for the subsequent sintering process.

After 55 hours of ball milling, the homogeneous mixture was subjected to controlled sintering in an electric chamber furnace (Nabertherm N31/H) at different temperatures (500°C, 600°C, 700°C, 800°C, 900°C, 1000°C, and 1100°C) for 1 hour at each temperature. Sintering is a critical step to tune the crystallite size, phase purity, and density of the PST material. The selected temperature range of 500°C to 1100°C was chosen based on prior studies on similar perovskites, such as $\text{Ba}_{0.6}\text{Sr}_{0.4}\text{TiO}_3$, where sintering in this range enhanced both the structural and electrical properties of the material [25].

At lower sintering temperatures (500°C–600°C), the process is governed by solid-state diffusion, with particle reorganization and minor densification. Controlling porosity at this stage is essential to avoid degradation of mechanical properties, which is vital for biomedical applications, where material strength and integrity are paramount. At intermediate temperatures (700°C–800°C), liquid-phase sintering becomes

Table 1. Properties of PbCO_3 , SrCO_3 , and TiO_2 .

Materials	Properties				
	Molecular Weight (g/mol)	Melting Point (°C)	Density (g/cm ³)	Decomposition Temperature (°C)	Ref.
PbCO_3	267	315	6.6	315	[22]
SrCO_3	147.63	1494	3.5	1100	[23]
TiO_2	79.8	1855	3.9-4.3	1860	[24]

predominant, leading to increased mass transport and densification. This phase is characterized by enhanced crystallinity, reduced porosity, and improved mechanical properties, critical for applications requiring structural integrity and dielectric performance. Sintering at 900°C to 1000°C results in nearly complete densification, further reducing porosity and optimizing the dielectric and ferroelectric properties of the PST material, making it suitable for high-performance biomedical sensors. Finally, sintering at 1100°C facilitates significant grain growth, which can further improve material properties relevant to biomedical devices [25–29].

XRD analysis [30] of the sintered products was performed using a Philips (Model PW 1835) powder diffractometer with Cu K α radiation ($\lambda = 0.15406$ nm) operating at 40 kV and 30 mA. Diffractograms were recorded over a 2θ range of 10° to 90° with a step size of 0.02° and a scan rate of 1°/min. Phase identification and quantification were achieved through Rietveld refinement using the High Score Plus software, employing the pseudo-Voigt function to model the diffraction line profiles. The crystallite sizes were calculated using the Williamson–Hall method, which accounts for both crystallite size broadening and strain-induced broadening in the diffraction peaks [31].

Particle size analysis of the raw materials and ball-milled products was conducted using a Laser Diffraction Particle Size Analyzer (LS-PSA, Beckman Coulter, U.S.A.) capable of measuring particle sizes in the range of 0.4 to 900 μm . The LS-PSA was connected to a computer equipped with LS Coulter 100 software, allowing for precise measurement and analysis of the particle size distribution of each sample. This analysis is critical for ensuring that the starting powders have suitable particle sizes for effective sintering and phase formation.

3. Results and discussion

3.1. Raw material and ball milling product characterization

The initial characterization of PbCO₃, SrCO₃, and TiO₂ powders was performed using a Particle Size Analyzer (PSA). The average particle sizes of the powders, summarized in Table 2, were measured at 1.33 μm for PbCO₃, 3.18 μm for SrCO₃, and 0.80 μm for TiO₂. These particle sizes reflect the starting conditions of the raw materials, which play a crucial role in the subsequent ball milling and sintering processes

aimed at tuning the crystallite size and phase purity for biomedical applications.

The XRD patterns of the individual raw materials, PbCO₃, SrCO₃, and TiO₂, are shown in Figure 1. These patterns confirm the crystalline phases of the raw materials, with PbCO₃, SrCO₃, and TiO₂ identified using ICSD numbers 98-016-6089, 98-016-6088, and 98-002-4276, respectively. No impurities or secondary phases were detected, ensuring the phase purity of the starting materials. The ball milling process was performed for durations ranging from 5 to 58 hours, with the particle size evolution recorded at different intervals. As illustrated in Figure 2, the particle size increased significantly during the first 5 to 10 hours of milling due to cold-welding, where particles coalesce, forming larger aggregates. However, as the milling time progressed beyond 10 hours, the particle size began to decrease, indicating the onset of the intermediate grinding phase, where repeated impacts and compression break down agglomerates into finer particles.

The ball milling process plays a crucial role in controlling the crystallite size and phase purity of Pb_{1-x}Sr_xTiO₃ ferroelectric perovskites, which are essential for optimizing their functional properties in biomedical applications. The process can generally be divided into three stages: agglomeration, intermediate, and homogenization [32,33]. During the initial stage (5–10 hours of milling), powder particles of PbCO₃, SrCO₃, and TiO₂ tend to agglomerate due to cold welding, leading to the formation of larger clusters [32,33]. This agglomeration stage is marked by an increase in particle size, which is observed in the mixture of PbCO₃, SrCO₃, and TiO₂. Such agglomeration can significantly affect the early phase of perovskite formation, potentially impacting the crystallization process during sintering and thus the resultant phase purity.

In the intermediate grinding stage (10–58 hours), the agglomerated particles are progressively broken down due to repeated impact and compression forces. The particle sizes at various milling durations (10, 25, 35, 45, 55, and 58 hours) were recorded as 17.51, 9.65, 4.08, 1.49, 0.61, and 0.61 μm , respectively. This reduction in particle size is critical, as smaller, uniform particles contribute to the formation of a well-ordered perovskite structure, enhancing crystallite size control and phase purity during subsequent sintering. The homogenization stage, observed at 55 and 58 hours of milling, resulted in a constant particle size of 0.61 μm , indicating that the mixture had reached a uniform state. This uniformity is particularly important for biomedical applications, where controlled crystallite sizes can affect material properties such as biocompatibility, dielectric constant, and piezoelectric behavior, making Pb_{1-x}Sr_xTiO₃ perovskites highly suitable for sensors and actuators in medical devices [18,20,34].

Table 2. Average particle size of raw materials.

Materials	Average particle size (μm)
PbCO ₃	1.33
SrCO ₃	3.18
TiO ₂	0.80

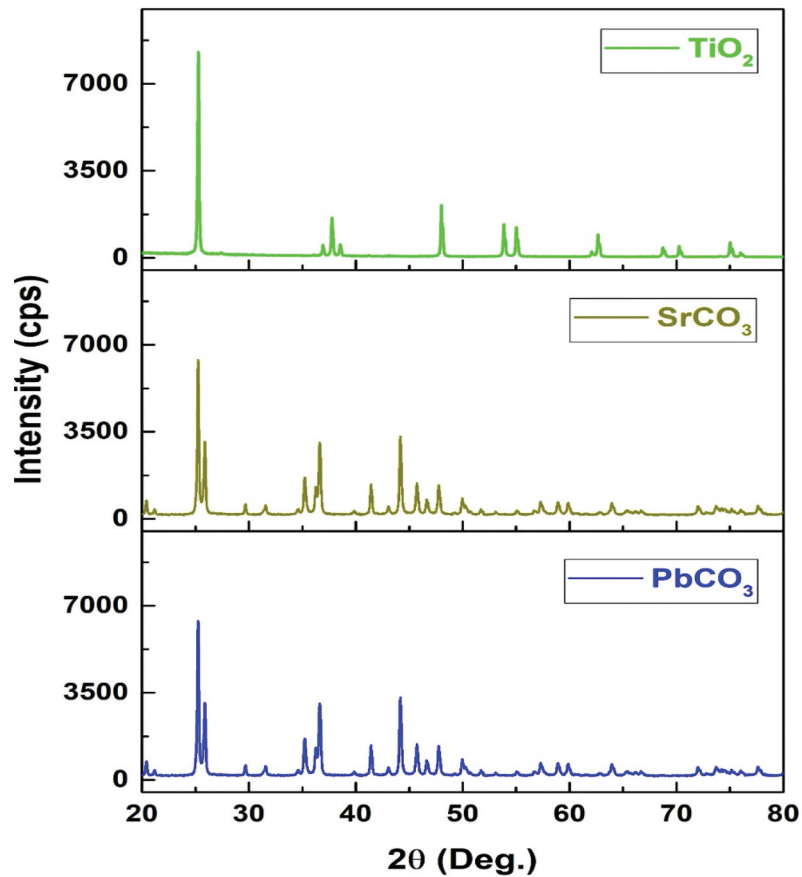


Figure 1. XRD patterns of the PbCO_3 , SrCO_3 , and TiO_2 from the inorganic crystal structure database.

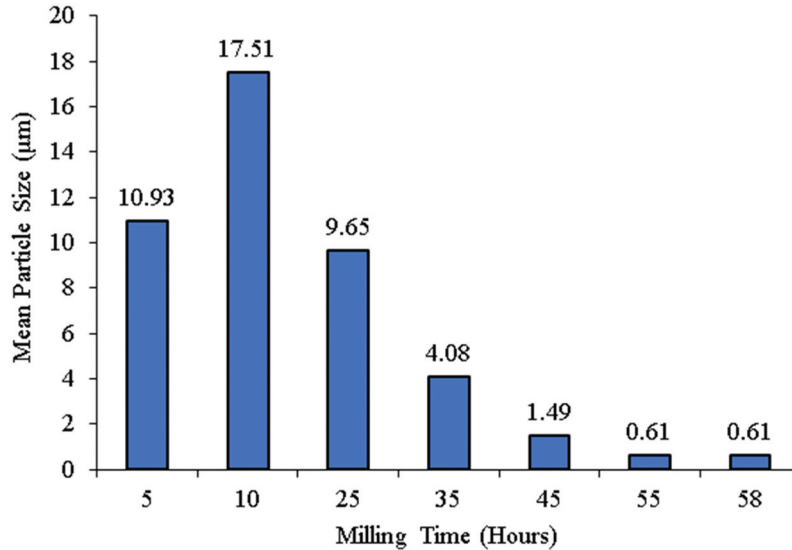


Figure 2. Effect of milling duration on particle size in mixtures of PbCO_3 , SrCO_3 , and TiO_2 .

These findings are consistent with previous studies. For instance, Tousei et al. [35] observed a similar agglomeration and particle size reduction in Al powder, with a significant size decrease occurring after 4 hours of milling. Likewise, El-Eskandarany et al. [36] reported a comparable trend for Fe₅₂Nb₄₈ alloy powder, where particle size initially increased during the first 20 hours of milling before decreasing, with optimal particle size achieved after 40 hours. The

continued reduction in particle size with prolonged milling in this study can be attributed to enhanced collisions between the milling balls and the raw material, resulting in more efficient size reduction and greater homogeneity in the mixture [37–40]. This fine and uniform powder is essential for achieving high phase purity in $\text{Pb}_{1-x}\text{Sr}_x\text{TiO}_3$ perovskites during the sintering process, which is critical for optimizing their performance in biomedical applications.

X-ray diffraction (XRD) analysis of the milled mixture of PbCO_3 , SrCO_3 , and TiO_2 for varying durations (5 hours, 10 hours, 25 hours, 35 hours, 45 hours, and 55 hours) is presented in Figure 3. The XRD patterns confirm the presence of all three starting compounds across all milling durations. The results indicate that extending the milling time leads to only minor changes in peak intensity, with no evidence of new phase formation, even after 55 hours of milling. This suggests that the structural integrity of the initial compounds is largely preserved during the ball milling process, while other mechanisms, such as crystallite size reduction and increased lattice strain, are at play. The effect of milling duration on the crystallite sizes of PbCO_3 , SrCO_3 , and TiO_2 is depicted in Figure 4.

The findings consistently show that increasing the milling duration leads to a reduction in the crystallite sizes of PbCO_3 , SrCO_3 , and TiO_2 . This is a critical observation for controlling the crystallite size of $\text{Pb}_{1-x}\text{Sr}_x\text{TiO}_3$ perovskites during sintering, where

smaller crystallites can enhance phase purity and functional properties that important for their application in biomedical devices such as piezoelectric sensors and actuators. The reduction in crystallite size aligns with the work of Sabrina et al. [41], who observed a significant decrease in the crystallite size of $\text{Fe}_{20}\text{Cr}_5\text{AlT}$ as mixing duration increased from 0 to 48 hours. This decrease is associated with the broadening of X-ray diffraction peaks due to an increase in the full width at half-maximum (FWHM), which is directly related to a reduction in crystallite size as milling time increases.

Similar findings have been reported by Rijesh et al. [42], who demonstrated that Al powders exhibited a continuous decrease in crystallite size as the ball milling duration increased, further reinforcing the relationship between milling time and reduced crystal size. Wong et al. [43] also observed that prolonged milling of SrCO_3 and TiO_2 mixtures led to a marked reduction in crystallite size, along with increased lattice strain and peak broadening. These

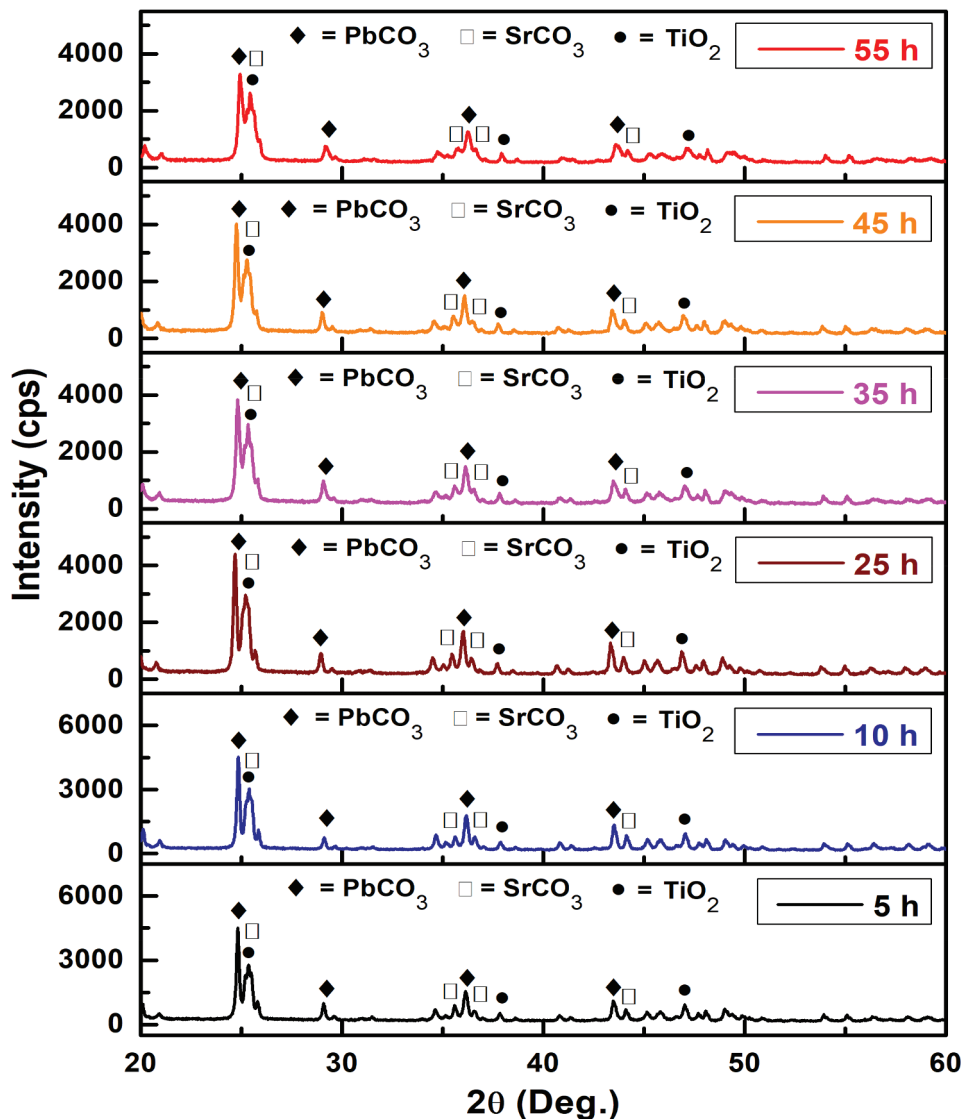


Figure 3. XRD patterns of the ball milling products.

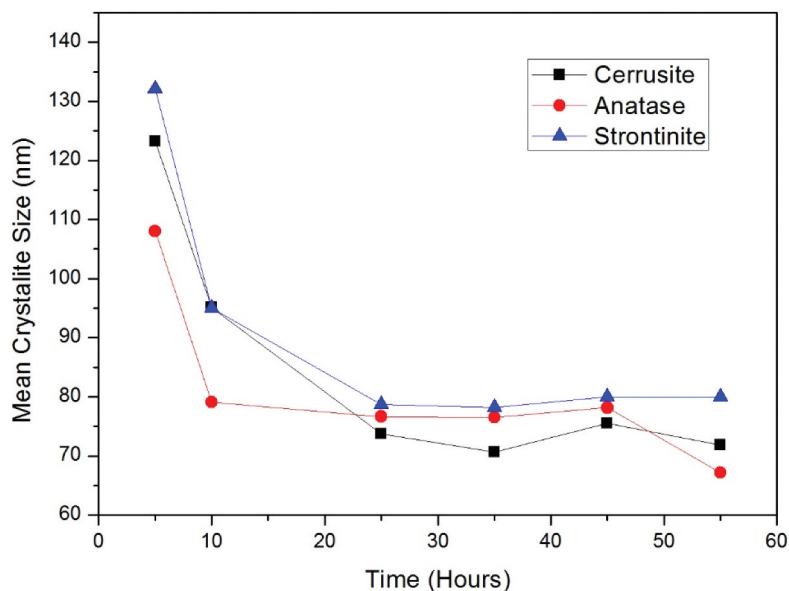


Figure 4. Effect of milling duration on crystal size in mixtures of PbCO_3 , SrCO_3 , and TiO_2 .

structural changes are attributed to the accumulation of lattice defects and increased mechanical strain during milling, which are critical factors in reducing crystallite size and tuning phase purity during sintering.

Moreover, the study by Rajkovic et al. [44] on Cu-2.5 wt%Al demonstrated that increased milling time resulted in significant reductions in crystal size, driven by enhanced lattice distortion and broader XRD peaks, consistent with the trend observed in this study. The inverse relationship between milling time and crystallite size, as well as the increasing lattice distortion with prolonged milling, is essential for the optimization of $\text{Pb}_{1-x}\text{Sr}_x\text{TiO}_3$ perovskite crystallites in biomedical applications, where precise control over crystallite size is needed to improve material performance and phase stability during sintering.

3.2. Sintering product characterization

Figure 5 illustrates the influence of sintering temperature on the formation of $\text{Pb}_{0.4}\text{Sr}_{0.6}\text{TiO}_3$ material, highlighting the temperature-dependent nature of the synthesis process. At lower temperatures (500°C and 600°C), the $\text{Pb}_{0.4}\text{Sr}_{0.6}\text{TiO}_3$ perovskite structure does not form, with the starting materials PbCO_3 , SrCO_3 , and TiO_2 remaining, indicating incomplete chemical reactions. As the sintering temperature increases from 700°C to 1000°C, the formation of $\text{Pb}_{0.4}\text{Sr}_{0.6}\text{TiO}_3$ is observed, although impurities persist in the resulting material. Notably, at a higher sintering temperature of 1100°C, pure $\text{Pb}_{0.4}\text{Sr}_{0.6}\text{TiO}_3$ is obtained, free from impurities. These findings underscore the critical role of sintering temperature in achieving phase purity and optimizing the properties of the material for biomedical applications.

The incorporation of strontium (Sr) significantly affects the crystal lattice of PbTiO_3 , where Sr^{2+} ions partially replace Pb^{2+} ions, resulting in the $\text{Pb}_{1-x}\text{Sr}_x\text{TiO}_3$ perovskite structure. Distinct peaks corresponding to the $\text{Pb}_{0.6}\text{Sr}_{0.4}\text{TiO}_3$ phase become increasingly pronounced at elevated sintering temperatures (900°C, 1000°C, and 1100°C). In contrast, at lower temperatures (500°C to 700°C), the stable perovskite phase with sufficient Sr substitution is not fully developed, indicating inadequate integration of Sr into the perovskite structure. The presence of secondary phases, such as SrCO_3 and TiO_2 , suggests that the chemical interactions among the components remain incomplete at these lower temperatures.

Conversely, at higher sintering temperatures (700°C and above), the peak intensities of the perovskite phases $\text{Pb}_{0.6}\text{Sr}_{0.4}\text{TiO}_3$ and PbTiO_3 begin to rise, while the intensity of secondary phases like SrCO_3 starts to diminish, especially beyond 900°C. Elevated sintering temperatures promote more thorough phase transitions and reduce the prevalence of secondary phases, enhancing ion diffusion and facilitating the effective incorporation of Sr into the perovskite structure. By 1100°C, the secondary phase is entirely absent, with $\text{Pb}_{0.6}\text{Sr}_{0.4}\text{TiO}_3$ emerging as the sole phase.

To quantify these changes, Rietveld analysis was performed using High Score Plus software, evaluating the effects of sintering temperature on the crystal system, phase composition, and crystallite size of $\text{Pb}_{0.4}\text{Sr}_{0.6}\text{TiO}_3$ crystals. A consistent cubic crystal structure was maintained across the sintering temperature range of 700°C to 1100°C (Figure 6). The phase composition of $\text{Pb}_{0.4}\text{Sr}_{0.6}\text{TiO}_3$ significantly increased with rising sintering temperatures, achieving values of 27.58%, 65.59%, 72.9%, 92.5%, and 100% at 700°C, 800°C, 900°C, 1000°C, and 1100°C, respectively.

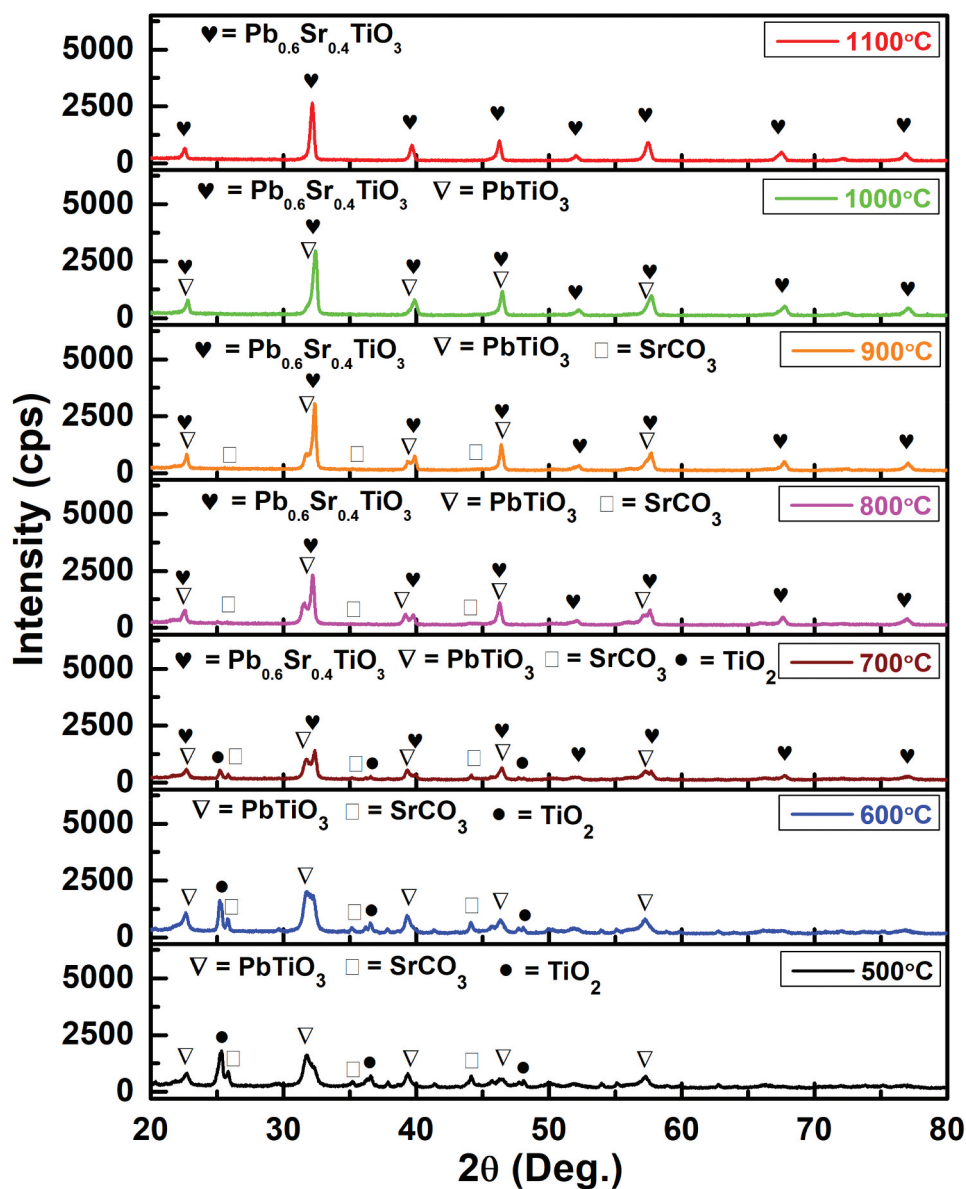


Figure 5. XRD patterns on specimens at various sintering temperatures.

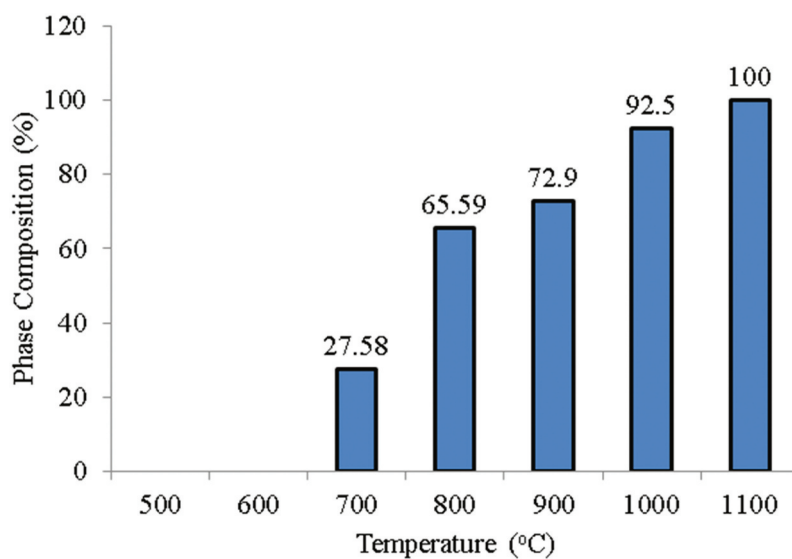


Figure 6. Effect of sintering temperature on phase composition (%) in $\text{Pb}_{0.4}\text{Sr}_{0.6}\text{TiO}_3$ crystals.

Notably, the formation of the $\text{Pb}_{0.4}\text{Sr}_{0.6}\text{TiO}_3$ phase was not observed at 500°C and 600°C.

This correlation between higher sintering temperatures and increased phase composition of $\text{Pb}_{0.4}\text{Sr}_{0.6}\text{TiO}_3$ is attributed to the higher kinetic energy of atoms at elevated temperatures, which facilitates enhanced atomic interactions and bonding, leading to the elimination of impurities [45,46]. Furthermore, the elevated sintering temperatures promote recrystallization in the precursor materials (PbCO_3 , SrCO_3 , and TiO_2) and foster crystal growth in the $\text{Pb}_{0.4}\text{Sr}_{0.6}\text{TiO}_3$ phase, resulting in a higher phase composition and improved material properties.

Previous studies have demonstrated that the $\text{Ba}_{0.6}\text{Sr}_{0.4}\text{TiO}_3$ phase initiates formation at a sintering temperature of 700°C, with pure $\text{Ba}_{0.6}\text{Sr}_{0.4}\text{TiO}_3$ material achieved at 1000°C [33]. Similarly, Sahu et al. [47] reported that increasing the sintering temperature leads to the elimination of impurity phases, resulting in a purer $\text{Al}_{86}\text{Ni}_6\text{Y}_{4.5}\text{CO}_2\text{La}_{1.5}$ composition. Their findings indicate that elevated sintering temperatures enhance viscous flow, facilitating the formation and subsequent disappearance of complex metastable phases during the sintering process. Additionally, Wang and Hu [48], Whiney et al. [49], and Laeng et al. [50] demonstrated that extending the sintering time and increasing the sintering temperature effectively reduces the percentages of NiTi_2 and Ni_3Ti impurities in NiTi alloys. Moreover, research by Fu et al. [51] concluded that elevating the sintering temperature to 800°C results in the complete disappearance of the impurity phases $\text{Bi}_2\text{Fe}_4\text{O}_9$, yielding a single-phase BiFeO_3 with a distorted perovskite structure.

The effect of sintering temperature on the crystallite size (in nanometers) of $\text{Pb}_{0.4}\text{Sr}_{0.6}\text{TiO}_3$ is depicted in Figure 7, demonstrating a clear trend where increased sintering temperatures correlate with enhanced crystal size. The measured crystallite sizes

were 62.1 nm, 74.2 nm, 134 nm, 98.3 nm, and 91.5 nm at sintering temperatures of 700°C, 800°C, 900°C, 1000°C, and 1100°C, respectively. These results indicate that the recrystallization mechanism and excessive grain growth at elevated temperatures facilitate size reduction, while the most substantial crystal growth occurs at 900°C, where the largest size of 134 nm was observed.

The growth in crystallite size with sintering temperatures of 700°C, 800°C, or 900°C can be attributed to increased atomic kinetic mobility, enhanced crystallinity, and higher levels of oxygen vacancies, which collectively promote crystallite growth during sintering. As the process progresses, the microstructure evolves from relatively compact particles to a dense, nearly pore-free structure. The bonding of particles involves atomic diffusion, which is facilitated by the increased atomic kinetic mobility at higher sintering temperatures, ultimately leading to crystallite growth [52–55].

Notably, an intriguing phenomenon occurs at sintering temperatures of 1000°C and 1100°C, where the crystallite size begins to decrease, measuring 98.3 nm and 91.5 nm, respectively, which is smaller than the size recorded at 900°C. This observation aligns with the findings of Nazarian-Samani et al. [56], who reported a similar trend in a nanocrystalline Ni_3A alloy, where increasing the sintering temperature up to 1000°C led to enhanced crystal size, but further elevation beyond 1000°C resulted in size reduction. This pattern underscores the complex relationship between sintering temperature and crystallite size, highlighting the importance of precise temperature control to achieve desired material characteristics.

Perovskite materials exhibit unique properties that can be further enhanced through a controlled sintering synthesis process, making them exceptionally suitable for a variety of applications, particularly in the

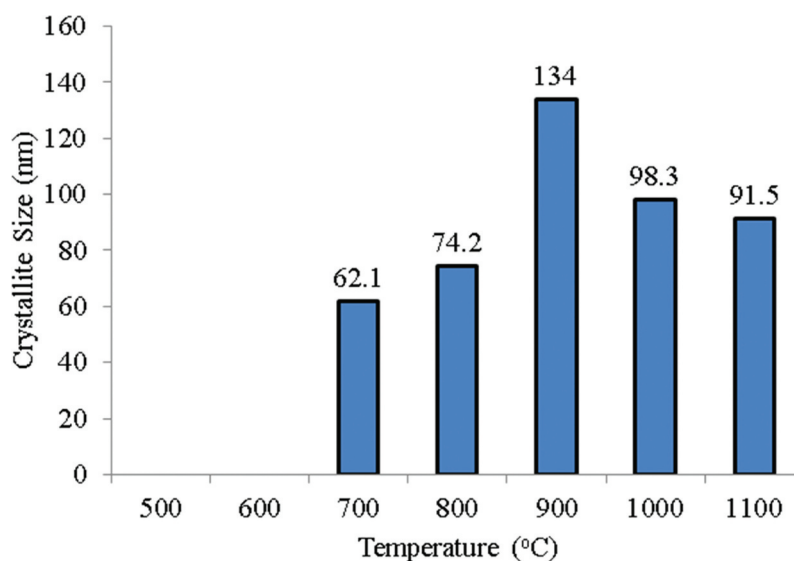


Figure 7. Effect of sintering temperature on crystal size of $\text{Pb}_{0.4}\text{Sr}_{0.6}\text{TiO}_3$.

biomedical field. Their piezoelectric and ferroelectric properties offer promising applications in biosensors [57], bioimaging [58], and light-activated therapeutics [59]. Furthermore, perovskite-based nanoparticles show potential for cancer treatment [60]. Their biocompatibility and mechanical robustness position them as optimal candidates for tissue engineering and orthopedic implants, especially lead-free perovskite materials, which are considered safer and more environmentally sustainable for medical applications [61].

4. Conclusions

This study investigated the influence of sintering temperature on the weight percentage and crystallite size of PST perovskites. The synthesis involved combining PbCO_3 , SrCO_3 , and TiO_2 powders through a solid-state reaction, with the powder mixing process utilizing vibratory ball milling divided into three stages: accumulation, intermediate, and homogenization. PSA revealed that during the agglomeration phase (5–10 hours), particle size increased due to interactions between neighboring particles. This was followed by fragmentation during the intermediate phase (10–58 hours), where repeated compression led to a more uniform particle size distribution. Notably, the particle size stabilized during the homogenization phase (55–58 hours). XRD analysis indicated that longer milling durations resulted in reduced particle sizes, attributed to increased lattice distortion and broadening of diffraction peaks. Temperature emerged as a critical factor in the synthesis of $\text{Pb}_{0.4}\text{Sr}_{0.6}\text{TiO}_3$, significantly affecting the phase composition and material properties. The phase composition of $\text{Pb}_{0.4}\text{Sr}_{0.6}\text{TiO}_3$ increased with rising sintering temperatures, reaching values of 27.58%, 65.59%, 72.9%, 92.5%, and 100% at 700°C, 800°C, 900°C, 1000°C, and 1100°C, respectively. No formation of the desired phase occurred at 500°C and 600°C, underscoring the necessity of optimal sintering conditions. The sintering treatment at 1100°C yielded the most favorable specimen, resulting in a fully pure and impurity-free PST. Analysis using High Score Plus software confirmed the temperature's role in influencing the crystal sintering system, phase composition, and crystallite size of $\text{Pb}_{0.4}\text{Sr}_{0.6}\text{TiO}_3$. A consistent cubic phase was observed within the 700–1000°C range, where high temperatures facilitated enhanced phase formation and impurity elimination. This improvement is attributed to the increased kinetic energy at elevated sintering temperatures, which promotes atom interactions and bond formation, thereby reducing impurity phases. Crystallization at higher temperatures led to increased crystallite sizes, with sizes of 62.1 nm, 74.2 nm, 134 nm, 98.3 nm, and 91.5 nm recorded at sintering temperatures of 700°C, 800°C, 900°C, 1000°C, and 1100°C, respectively. A marked increase in crystallite

size was noted from 700°C to 900°C, peaking at 134 nm due to enhanced atomic mobility, improved crystallinity, and the presence of oxygen vacancies. However, a decline in size at sintering temperatures of 1000°C and 1100°C indicates the complexity of the relationship between temperature and crystallite size. Precise control over the sintering temperature is crucial for tailoring the crystallite size and phase purity of $\text{Pb}_{0.4}\text{Sr}_{0.6}\text{TiO}_3$ ferroelectric perovskites, optimizing them for biomedical applications. These findings provide valuable insights for enhancing the manufacturing processes of perovskite materials, promoting the production of high-quality materials suitable for a range of biomedical applications.

Acknowledgments

The authors gratefully thank their respective institutions for their strong support in this study.

Disclosure statement

No potential conflict of interest was reported by the author(s).

Funding

This research is fully supported by the Faculty of Engineering, Universitas Negeri Semarang, Indonesia, with Research Grant-No: [151.22.3/UN37/PPK.05/2024].

ORCID

Rahmat Doni Widodo  <http://orcid.org/0000-0002-9750-6811>

Samsudin Anis  <http://orcid.org/0000-0003-4414-544X>


Deni Fajar Fitriyana  <http://orcid.org/0000-0002-5287-6122>

Maykel Manawan  <http://orcid.org/0000-0003-3782-1307>

Joni Sah  <http://orcid.org/0009-0009-4646-6002>

Rizalman Bin Mamat  <http://orcid.org/0000-0002-6562-0994>

Abdulfatah Abdu Yusuf  <http://orcid.org/0000-0002-8054-9022>

Muhammad Imam Ammarullah  <http://orcid.org/0000-0002-8845-7202>

Author contribution

The authors have significantly contributed to the development and the writing of this article.

Additional information

No additional information is available for this paper.

Consent for publication

The authors consent to the publication of this manuscript.

CRediT statement

Rahmat Doni Widodo: Conceptualization, Data curation, Formal analysis, Funding acquisition, Investigation, Methodology, Project administration, Resources, Software, Supervision, Validation, Visualization, Writing – original draft, Writing – review & editing. **Samsudin Anis:** Conceptualization, Data curation, Formal analysis, Funding acquisition, Investigation, Methodology, Project administration, Resources, Software, Supervision, Validation, Visualization, Writing – original draft, Writing – review & editing. **Deni Fajar Fitriyana:** Conceptualization, Data curation, Formal analysis, Funding acquisition, Investigation, Methodology, Project administration, Resources, Software, Supervision, Validation, Visualization, Writing – original draft, Writing – review & editing. **Maykel Manawan:** Conceptualization, Data curation, Formal analysis, Funding acquisition, Investigation, Methodology, Project administration, Resources, Software, Supervision, Validation, Visualization, Writing – original draft, Writing – review & editing. **Joni Sah:** Conceptualization, Data curation, Formal analysis, Funding acquisition, Investigation, Methodology, Project administration, Resources, Software, Supervision, Validation, Visualization, Writing – original draft, Writing – review & editing. **Aji Santiko:** Conceptualization, Data curation, Formal analysis, Funding acquisition, Investigation, Methodology, Project administration, Resources, Software, Supervision, Validation, Visualization, Writing – original draft, Writing – review & editing. **Rizalman Bin Mamat:** Conceptualization, Data curation, Formal analysis, Funding acquisition, Investigation, Methodology, Project administration, Resources, Software, Supervision, Validation, Visualization, Writing – original draft, Writing – review & editing. **Abdulfatah Abdu Yusuf:** Conceptualization, Data curation, Formal analysis, Funding acquisition, Investigation, Methodology, Project administration, Resources, Software, Supervision, Validation, Visualization, Writing – original draft, Writing – review & editing. **Muhammad Imam Ammarullah:** Conceptualization, Data curation, Formal analysis, Funding acquisition, Investigation, Methodology, Project administration, Resources, Software, Supervision, Validation, Visualization, Writing – original draft, Writing – review & editing.

Data availability statement

The necessary data used in the manuscript are already present.

Ethical Statement

This study did not involve human participants or animals, and no ethical approval was required. All research procedures adhered to relevant ethical guidelines and best practices for non-human and non-animal research.

Statement of originality

The authors declare that this manuscript is original, has not been published before and is not currently being considered for publication elsewhere. The authors confirm that the manuscript has been read and approved by all named authors and that there are no other persons who satisfied the criteria for authorship but are not listed. The authors further confirm that the order of authors listed in the

manuscript has been approved by all of us. The authors understand that the corresponding author is the sole contact for the Editorial process. The corresponding author is responsible for communicating with the other authors about progress, submissions of revisions and final approval of proofs.

Transparency statement

The authors affirm that this manuscript is an honest, accurate, and transparent account of the study being reported; that no important aspects of the study have been omitted; and that any discrepancies from the study as planned (and, if relevant, registered) have been explained.

Declaration of AI use

The authors declare not use AI-assisted technologies in creating this article.

References

- [1] Z Q, Arne Lüker PBK, and Ferroelectrics QZ, editor. The effect of Mn doping on the dielectric properties of lead strontium titanate (PST). Rijeka: IntechOpen; 2011. p. 9. doi: [10.5772/21872](https://doi.org/10.5772/21872)
- [2] Wang X, Zhang L, Liu H, et al. Dielectric nonlinear properties of BaTiO₃–CaTiO₃–SrTiO₃ ceramics near the solubility limit. *Mater Chem Phys*. 2008;112(2):675–678. doi: [10.1016/j.matchemphys.2008.06.020](https://doi.org/10.1016/j.matchemphys.2008.06.020)
- [3] Kumar A, Chandkiram Y. Dielectric behavior of perovskite glass ceramics. *J Mater Sci Mater Electron*. 2014;25(12):5165–5187. doi: [10.1007/s10854-014-2311-6](https://doi.org/10.1007/s10854-014-2311-6)
- [4] Sittiketkorn P, Bongkarn T. The preparation of lead strontium titanate ceramics by the combustion method the preparation of lead strontium titanate. *Ferroelectrics*. 2011;414(1):170–179. doi: [10.1080/00150193.2011.577335](https://doi.org/10.1080/00150193.2011.577335)
- [5] Jain M, Majumder SB, Guo R, et al. Synthesis and characterization of lead strontium titanate thin films by sol-gel technique. *Mater Lett*. 2002;56(5):692–697. doi: [10.1016/S0167-577X\(02\)00597-9](https://doi.org/10.1016/S0167-577X(02)00597-9)
- [6] Tang ZX, Ge PZ, Tang XG, et al. Pyroelectric energy harvesting and ferroelectric properties of PbxSr1-xTiO3 ceramics. *J Asian Ceram Soc*. 2020;8(4):1147–1153. doi: [10.1080/21870764.2020.1824317](https://doi.org/10.1080/21870764.2020.1824317)
- [7] Sittiketkorn P, Bongkarn T. The preparation of lead strontium titanate ceramics by the combustion method. *Ferroelectrics*. 2011;414(1):170–179. doi: [10.1080/00150193.2011.577335](https://doi.org/10.1080/00150193.2011.577335)
- [8] Chen P, Pan H, Chou C, et al. Microstructures and properties of semi-conductive Pb_{0.6}Sr_{0.4}TiO₃ ceramics using PbTiO₃-coated SrTiO₃ powders. *J Eur Ceram Soc*. 2001;21(10–11):1905–1908. doi: [10.1016/S0955-2219\(01\)00140-6](https://doi.org/10.1016/S0955-2219(01)00140-6)
- [9] Jiang Y, Tang X, Zhou Y, et al. Structure and composition-dependent optical properties of (PbxSr1-x)TiO3 (x=0.4, 0.6) nanotube arrays. *Prog ini Nat Sci Mater Int*. 2011;21(3):198–204. doi: [10.1016/S1002-0071\(12\)60030-6](https://doi.org/10.1016/S1002-0071(12)60030-6)
- [10] Huang S, Chen J, Cheng J. Fabrication and characterization of compositionally graded PbxSr1-xTiO3 thin films on stainless steel by the Sol-gel method. *IEEE Int Symp Appl Ferroelectr Int Work Acoust Transduct Mater Devices Work Piezoresponse Force Microsc*. 2014:1–4. doi: [10.1109/isaf.2014.6922980](https://doi.org/10.1109/isaf.2014.6922980)

- [11] Jain M, Karan NK, Yoon J, et al. High tunability of lead strontium titanate thin films using a conductive LaNiO₃ as electrodes. *Appl Phys Lett*. 2007;91(7):35–38. doi: [10.1063/1.2770962](https://doi.org/10.1063/1.2770962)
- [12] Jain F, Yuzyuk YI, Katiyar RS, et al. Investigations of Pb_xSr_{1-x}TiO₃ thin films and ceramics for microelectronic applications. *MRS Online Proceedings Library*. 2004;811:1–6. doi: [10.1557/PROC-811-D3.36](https://doi.org/10.1557/PROC-811-D3.36)
- [13] Zhai J, Yao X, Xu Z, et al. Ferroelectric properties of Pb_xSr_{1-x}TiO₃ and its compositionally graded thin films grown on the highly oriented LaNiO₃ buffered Pt/Ti/SiO₂/Si substrates. *J Appl Phys*. 2006 Aug;100(3):34108. doi: [10.1063/1.2234554](https://doi.org/10.1063/1.2234554)
- [14] Zhang F, Karaki T, Adachi M. Synthesis of nanosized (Pb,Sr)TiO₃ perovskite powders by coprecipitation processing. *Powder Technol*. 2005;159(1):13–16. doi: [10.1016/j.powtec.2005.04.056](https://doi.org/10.1016/j.powtec.2005.04.056)
- [15] Tzu TW, Sato K, Mohd Noor AF. Solid state synthesis of barium strontium titanate at 850 o C from mechanically activated BaCO₃-SrCO₃-TiO₂ mixture. *Proceeding of Malaysia-Japan International Symposium On Advanced Technology 2007 (MJISAT 2007)*. 2007.
- [16] Cho S-J, Uddin M-J, Alaboina P. In: *Micro Nano Technologies*, L. M. Rodriguez-Martinez, N. B. T.-E. N. in R. E. S. S Omar, editors. Chapter three - review of nanotechnology for cathode materials in batteries. Boston: Elsevier; 2017. p. 83–129. doi: [10.1016/B978-0-323-42977-1.00003-0](https://doi.org/10.1016/B978-0-323-42977-1.00003-0)
- [17] Li DH, He SF, Chen J, et al. Solid-state chemical reaction synthesis and characterization of lanthanum tartrate nanocrystallites under ultrasonication spectra. *IOP Conf Ser: Mater Sci Eng*. 2017;242(1):012023. doi: [10.1088/1757-899X/242/1/012023](https://doi.org/10.1088/1757-899X/242/1/012023)
- [18] Nesterov O. Control of periodic ferroelastic domains in ferroelectric Pb_{1-x}Sr_xTiO₃ thin films for nano-scaled memory devices. Netherlands: University of Groningen; 2015.
- [19] Jain M, Savvinov A, Dobal PS, et al. Structural and Vibrational Properties of Ferroelectric Pb_{1-x}Sr_xTiO₃ Thin Films and Powders. *MRS Online Proceedings Library*. 2002;748:317. doi: [10.1557/PROC-748-U3.17](https://doi.org/10.1557/PROC-748-U3.17)
- [20] Sumang R, Bongkarn T. Effect of sintering temperature on the crystal structure, microstructure and phase transition of (pb_{1-x}Sr_x)TiO₃ ceramics. *Funct Mater Lett*. 2009;2(4):193–197. doi: [10.1142/S179360470900079X](https://doi.org/10.1142/S179360470900079X)
- [21] Kim K, Kim C, Lee S. Dielectric properties of (pb, Sr) TiO₃ thin films prepared by using the sol-gel method. *J Korean Phys Soc*. 2002;41(3):377–380.
- [22] National Center for Biotechnology Information. PubChem Compound Summary for CID 11727, Lead carbonate. 2022 11 Sep. <https://pubchem.ncbi.nlm.nih.gov/compound/Lead-carbonate>
- [23] National Center for Biotechnology Information. PubChem compound summary for CID 15407, strontium carbonate. 2022 [cited 2022 Sep 11]. <https://pubchem.ncbi.nlm.nih.gov/compound/Strontium-carbonate>
- [24] National Center for Biotechnology Information. PubChem compound summary for CID 26042, titanium dioxide. 2022 [cited 2022 Sep 11]. Available from: <https://pubchem.ncbi.nlm.nih.gov/compound/Titanium-dioxide>
- [25] Rusiyanto R, Widodo RD, Al-Janani DH, et al. Effect of sintering temperature on the physical properties of Ba_{0.6}Sr_{0.4}TiO₃ prepared by solid-state reaction. *Int J Automot Mech Eng*. 2021 Jun;18(2):8752–8759. doi: [10.15282/ijame.18.2.2021.13.0669](https://doi.org/10.15282/ijame.18.2.2021.13.0669)
- [26] Caro CTG, Figueroa IA, Verduzco JA, et al. Solid state transformations from spheres to polyhedra in hollow Fe spheres. *Rev Mex Fis*. 2023;69(5):1–11. doi: [10.31349/RevMexFis.69.051001](https://doi.org/10.31349/RevMexFis.69.051001)
- [27] Yahya H, Othman MR, Ahmad ZA. Effect of the firing temperature on mechanical and physical properties of porcelain balls as grinding media. *Mater Sci Forum*. 2017;888 MSF, pp. 37–41. doi: [10.4028/www.scientific.net/MSF.888.37](https://doi.org/10.4028/www.scientific.net/MSF.888.37)
- [28] Wei G, Luo F, Miao Y, et al. Treatment of zeolite adsorbed material as a potential nuclear waste glass-ceramic matrix. *J Am Ceram Soc*. 2022;105(1):257–267. doi: [10.1111/jace.18094](https://doi.org/10.1111/jace.18094)
- [29] Felege GN, Gurao NP, Upadhyaya A. Evolution of microtexture and microstructure during sintering of copper. *Metall Mater Trans A Phys Metall Mater Sci*. 2019;50(9):4193–4204. doi: [10.1007/s11661-019-05317-7](https://doi.org/10.1007/s11661-019-05317-7)
- [30] Santoso B, Ammarullah MI, Haryati S, et al. Power and energy optimization of carbon based lithium-ion battery from water spinach (ipomoea aquatica). *J Ecol Eng*. 2023;24(3):213–223. doi: [10.12911/22998993/158564](https://doi.org/10.12911/22998993/158564)
- [31] Fitriyana DF, Ismail R, Bayuseno AP, et al. Characterization of hydroxyapatite extracted from crab shell using the hydrothermal method with varying holding times. *J Renew Mater*. 2024;12(6):1–19. doi: [10.32604/jrm.2024.052165](https://doi.org/10.32604/jrm.2024.052165)
- [32] Chen D, Jiang Y, Cai J-G, et al. 7 - production of intermetallic compound powders by a mechanochemical approach: solid-liquid reaction ball milling. In: M. B. T.-H.-E. B. M. Sopicka-Lizer, editor. *High-energy ball milling mechanochemical processing of nanopowders*. Woodhead Publishing; 2010. p. 149–166. doi: [10.1533/9781845699444.2.149](https://doi.org/10.1533/9781845699444.2.149)
- [33] Burmeister CF, Kwade A. Process engineering with planetary ball mills. *Chem Soc Rev*. 2013 Sep;42(18):7660–7667. doi: [10.1039/c3cs35455e](https://doi.org/10.1039/c3cs35455e)
- [34] Zhang L, Huang Z, Liu Y, et al. Effects of mechanical ball milling time on the microstructure and mechanical properties of Mo₂NiB₂-Ni Cermets. *Mater*. (Basel, Switzerland), vol. Materials. 2019 Jun;12(12):1–17. doi: [10.3390/ma12121926](https://doi.org/10.3390/ma12121926)
- [35] Razavi-Tousi SS, Szpunar JA. Role of ball milling of aluminum powders in promotion of aluminum-water reaction to generate hydrogen. *Metall Mater Trans E*. 2014;1(3):247–256. doi: [10.1007/s40553-014-0024-7](https://doi.org/10.1007/s40553-014-0024-7)
- [36] Sherif El-Eskandarany M, Bahgat AA, Gomaa NS, et al. Kinetics and formation mechanism of amorphous Fe₅₂Nb₄₈ alloy powder fabricated by mechanical alloying. *J Alloys Compd*. 1999;290(1–2):181–190. doi: [10.1016/s0925-8388\(99\)00222-4](https://doi.org/10.1016/s0925-8388(99)00222-4)
- [37] Sarimai S, Ratnawulan R, Ramli R, et al. Effect of milling time on particle size of forsterite (Mg₂SiO₄) from South Solok District. *IOP Conf Ser Mater Sci Eng*. 2018;335(1):1–6. doi: [10.1088/1757-899X/335/1/012004](https://doi.org/10.1088/1757-899X/335/1/012004)
- [38] Mukhtar NZF, Borhan MZ, Rusop M, et al. Effect of milling time on particle size and surface morphology of commercial zeolite by planetary ball mill. *Adv Mater Res*. 2013;795:711–715. doi: [10.4028/www.scientific.net/AMR.795.711](https://doi.org/10.4028/www.scientific.net/AMR.795.711)
- [39] Panigrahi N, Chaini R, Nayak A, et al. Impact of milling time and method on particle size and surface morphology during nano particle synthesis from α-Al₂O₃.

- Mater Today Proc. 2018;5(9):20727–20735. doi: [10.1016/j.matpr.2018.06.457](https://doi.org/10.1016/j.matpr.2018.06.457)
- [40] Prasoetsopha N, Pinitsoontorn S, Kamwanna T, et al. Effect of ball-milling time on particle size of $\text{Ca}_3\text{Co}_4\text{O}_9 + \delta$. Chiang Mai Univ J Nat Sci. 2014;13(2):635–643. doi: [10.12982/cmujns.2014.0065](https://doi.org/10.12982/cmujns.2014.0065)
- [41] Sabrina Q, Afandi A, Majid N. The effect of milling time on crystal size Sandvik Sanergy. J Nat Sci Math Res. 2020;6(1):12–16. doi: [10.21580/jnsmr.2020.6.1.11153](https://doi.org/10.21580/jnsmr.2020.6.1.11153)
- [42] Rijesh M, Sreekanth MS, Deepak A, et al. Effect of milling time on production of aluminium nanoparticle by high energy ball milling. Int J Mech Eng Technol. 2018;9(8):646–652.
- [43] Wong YJ, Jumiah H, Hashim M, et al. Effect of milling time on microstructure, crystallite size and dielectric properties of SrTiO_3 ceramic synthesized via mechanical alloying method. Adv Mater Res. 2012;364:388–392. doi: [10.4028/www.scientific.net/AMR.364.388](https://doi.org/10.4028/www.scientific.net/AMR.364.388)
- [44] Rajkovic V, Romhanji E, Mitkov M. Characterization of high-energy ball milled prealloyed copper powder containing 2.5 wt%Al. J Mater Sci Lett. 2002;21(2):169–173. doi: [10.1023/A:1014209618494](https://doi.org/10.1023/A:1014209618494)
- [45] Mudinepalli VR, Feng L, Lin W-C, et al. Effect of grain size on dielectric and ferroelectric properties of nanostructured $\text{Ba}_{0.8}\text{Sr}_{0.2}\text{TiO}_3$ ceramics. J Adv Ceram. 2015;4(1):46–53. doi: [10.1007/s40145-015-0130-8](https://doi.org/10.1007/s40145-015-0130-8)
- [46] Gatea HA, Naji IS. Impact of sintering temperature on structural and dielectric properties of barium strontium titanate prepared by sol-gel method. J Ovonic Res. 2018;14(6):467–474.
- [47] Sahu A, Maurya RS, Laha T. Effect of sintering temperature on phase evolution of $\text{Al}_{186}\text{Ni}_{6}\text{Y}_{4.5}\text{Co}_{2}\text{La}_{1.5}$ bulk amorphous composites synthesized via mechanical alloying and spark plasma sintering. Prog Nat Sci Mater Int. 2019;29(1):32–40. doi: [10.1016/j.pnsc.2019.01.009](https://doi.org/10.1016/j.pnsc.2019.01.009)
- [48] Wang J, Hu K. Phase transformation of NiTi alloys during vacuum sintering, IOP Conf. Ser Mater Sci Eng. 2017;204(1):1–5. doi: [10.1088/1757-899X/204/1/012023](https://doi.org/10.1088/1757-899X/204/1/012023)
- [49] Whitney M, Corbin SF, Gorbet RB. Investigation of the mechanisms of reactive sintering and combustion synthesis of NiTi using differential scanning calorimetry and microstructural analysis. Acta Mater. 2008;56(3):559–570. doi: [10.1016/j.actamat.2007.10.012](https://doi.org/10.1016/j.actamat.2007.10.012)
- [50] Laeng J, Xiu Z, Xu X, et al. Phase formation of Ni-Ti via solid state reaction. Phys Scr. 2007;T129:250–254. doi: [10.1088/0031-8949/2007/T129/056](https://doi.org/10.1088/0031-8949/2007/T129/056)
- [51] Fu C, Long X, Cai W, et al. Effect of sintering temperature on the microstructures and ferroelectric properties of bismuth ferrite ceramics. Ferroelectrics. 2013;445(1):114–120. doi: [10.1080/00150193.2013.814474](https://doi.org/10.1080/00150193.2013.814474)
- [52] Zangina T, Hassan J, Matori KA, et al. Sintering behavior, ac conductivity and dielectric relaxation of $\text{Li}_{1.3}\text{Ti}_{1.7}\text{Al}_{0.3}(\text{PO}_4)_3$ NASICON compound. Results Phys. 2017;6, no. March 719–725, no. March, doi: [10.1016/j.rinp.2016.10.003](https://doi.org/10.1016/j.rinp.2016.10.003)
- [53] Shah NA. Size induced tuning of dielectric behavior in nanostructured $\text{Y}_{0.95}\text{Ca}_{0.05}\text{MnO}_3$ compounds. Appl Nanosci. 2014;4(7):889–895. doi: [10.1007/s13204-013-0272-3](https://doi.org/10.1007/s13204-013-0272-3)
- [54] Głuchowski P, Tomala R, Kujawa D, et al. Insights into the relationship between crystallite size, sintering pressure, temperature sensitivity, and persistent luminescence color of $\text{Gd}_{2.97}\text{Pr}_{0.03}\text{Ga}_3\text{Al}_{20}\text{I}_{12}$ Powders and ceramics. J Phys Chem C. 2022;126(16):7127–7142. doi: [10.1021/acs.jpcc.2c00672](https://doi.org/10.1021/acs.jpcc.2c00672)
- [55] Singh LK, Bhadauria A, Jana S, et al. Effect of sintering temperature and heating rate on crystallite size, densification behaviour and mechanical properties of Al-mwcnt nanocomposite consolidated via spark plasma sintering. Acta Metall. Sin. (Engl. Lett.). 2018;31(10):1019–1030. doi: [10.1007/s40195-018-0795-4](https://doi.org/10.1007/s40195-018-0795-4)
- [56] Nazarian-Samani M, Kamali AR. Characteristics of thermal transitions during annealing of a nanocrystalline Ni3Al-based alloy. J Alloys Compd. 2009;486(1–2):315–318. doi: [10.1016/j.jallcom.2009.06.130](https://doi.org/10.1016/j.jallcom.2009.06.130)
- [57] Korde VB, Khot S, Kamble DB, et al. Review: perovskite nanostructures materials versatile platform for advance biosensor applications. Sensors Actuators Rep. 2024;7:100201. doi: [10.1016/j.snr.2024.100201](https://doi.org/10.1016/j.snr.2024.100201)
- [58] Gong J and Xu T. Perovskite materials in biomedical applications. In: N. S. Arul and V. D. Nithya, editors. Revolution of Perovskite: synthesis, properties and applications. Singapore: Springer Singapore; 2020. p. 95–116. doi: [10.1007/978-981-15-1267-4_4](https://doi.org/10.1007/978-981-15-1267-4_4)
- [59] Getachew G, Wibrianto A, Rasal AS, et al. Metal halide perovskite nanocrystals for biomedical engineering: recent advances, challenges, and future perspectives. Coord Chem Rev. 2023;482:1–43. doi: [10.1016/j.ccr.2023.215073](https://doi.org/10.1016/j.ccr.2023.215073)
- [60] Mishra D. In: S. Moharana, T. Badapanda, S. K. Satpathy, R. N. Mahaling R. B. T.-P. M. O. Kumar, editors. 15 - biomedical applications of perovskite-based materials, in Metal Oxides. Elsevier; 2023. p. 367–393. doi: [10.1016/B978-0-323-99529-0.00011-4](https://doi.org/10.1016/B978-0-323-99529-0.00011-4)
- [61] Chauhan V, Tripathi D, Singh P, et al. Prospects for lead free perovskite for photovoltaic applications and biological impacts: challenges and opportunities. Inorg Chem Commun. 2023;157:1–18. doi: [10.1016/j.inoche.2023.111421](https://doi.org/10.1016/j.inoche.2023.111421)